Regular Article

PHYSICAL CHEMISTRY RESEARCH
Published by the
Iranian Chemical Society
www.physchemres.org
info@physchemres.org

Phys. Chem. Res., Vol. 9, No. 2, 281-299, June 2021
DOI: 10.22036/pcr.2021.248702.1835

Surface Modification of $BiVO_4$ Using (3-Aminopropyl) Triethoxysilane and Study of the Photocatalytic Properties and Process Optimization

A. Mostajabi Gonabad[a], R. Fazaeli[a,*], I. Naser[a] and H. Pahlavan Zadeh[b]

[a]*Department of Chemical Engineering, Faculty of Engineering, South Tehran Branch, Islamic Azad University, Tehran, Iran*

[b]*Department of Chemical Engineering, Tarbiat Modares University, Tehran, Iran*

(Received 16 September 2020, Accepted 7 February 2021)

This research examined the photocatalytic degradation of oily pollutant, $BiVO_4$ with efficient photocatalytic activities synthesized *via* hydrothermal method with its surface modified by (3-aminopropyl) triethoxysilane (APTES). The structural, morphological, and optical properties of the as synthesized samples were evaluated by X-ray powder diffraction, scanning electron microscopy, energy-dispersive X-ray spectroscopy, contact angle, thermo gravimetric analysis, Fourier-transform infrared spectroscopy, UV-Vis diffuse reflectance spectroscopy, and analysis Brunauer-Emmett-Teller. The photocatalytic efficiency of the prepared samples was evaluated by Kerosine degradation. The experiments were designed by the Box-Behnken method. Finally, the software is the best point for achieving the highest percentage of degradation of oily pollutant under optimal conditions with pollutant concentration of 436.32 ppm, time of 2.62 h, catalyst mass of 0.77 g and H_2O_2 concentration of 0.42 M.

Keywords: $BiVO_4$, (3-Aminopropyl) triethoxysilane, Oily pollutant, Degradation, COD

INTRODUCTION

After the industrial revolution, environmental pollution and energy crisis have become serious challenges for humankind [1]. As a green chemistry technology [2], photocatalysis has been considered not only a cost-effective technology for decomposing organic pollutants into harmless chemicals but also as a promising alternative for solar energy utilization to solve these problems [2-6]. TiO_2 is the most widely and most promising photocatalyst used. Its high oxidation capacity, non-toxicity, as well as high chemical and biological stability are some of the characteristics making it superior to other kinds of photocatalytic materials. However, in practical applications TiO_2 is limited for its low utilization of solar energy, responding only to ultraviolet light, capturing only 4% of the sunlight energy. Nowadays, new materials with photocatalytic properties are being investigated for their effective utilization of the visible light energy. Generally, these materials are oxides based on metal cations with d_0 or d_{10} configurations, described as $A_xB_yO_z$. These metallates have been reported to take advantage of visible light more efficiently than conventional photocatalysts such as TiO_2 [6-9]. Among them, many new visible-light-induced photocatalysts such as A_gVO_x, Bi_2WO_6, Bi_2MO_6, Bi_2O_3, $CaBi_2O_4$, Bi_5O_7I, $InMO_4$ (M = V, Nb, Ta) or MIn_2O_4 (M = Ca, Sr, Ba) have also been reported. It is widely accepted that the properties of these materials depend on their crystal structure including tetragonal zircon, monoclinic and tetragonal scheelite structures. These crystalline forms can be synthesized via different preparation routes which allow obtaining the mentioned structures selectively depending on the preparation method. Bismuth vanadate ($BiVO_4$) is one of these visible-light

*Corresponding author. E-mail: r_fazaeli@azad.ac.ir

driven semiconductor photocatalysts being widely studied due to its steep absorption edges in the visible-light region. $BiVO_4$ can degrade organic pollutants and evolve O_2 and H_2 under visible light. In spite of this, it is still necessary to explore suitable semiconductors to combine with $BiVO_4$ and remarkably improve the photocatalytic activity [10,11]. Another type of wide band-gap bismuth salt, $BiPO_4$, only exhibits superior photocatalytic ability for organic dye decomposition in the UV region, which dramatically limits its practical applications [12]. APTES is frequently used as a coupling agent for attaching organic molecules to hydroxylated silicon oxide or metal oxide substrates, due to the presence of the terminal amine group on the propyl chain. Surface modification confers novel properties to nanoparticle surface, and influence the interaction of these particles and decrease the aggregation. Pirhashemi *et al.* studied the criteria anticipated for the fabrication of highly efficient ZnO-based visible-light-driven photocatalysts [13]. Akhundi *et al*. studied photocatalytic conversion of carbon dioxide to value-added compounds and renewable fuels by graphitic carbon nitride-based photocatalysts [14]. Akhundi *et al*. investigated graphitic carbon nitride-based photocatalysts: Toward efficient organic transformation for value-added chemicals production [15]. Asadzadeh-Khaneghah and Habibi-Yangjeh investigated g-C_3N_4/carbon dot-based nanocomposites as efficacious photocatalysts for environmental purification and energy generation [16]. In this study, $BiVO_4$ photocatalyst was synthesized by the hydrothermal method and its surface was modified by APTES to method of high temperature reactions with silane coupling agents [17,18]. The RSM method was used to evaluate the effective parameters and optimize the process of removing oily pollutant [19,20]. Also, isothermal and kinetic studies were performed and reported.

EXPERIMENTAL

Materials

Bismuth(III) nitrate pentahydrate $Bi(NO_3)_3{\cdot}5H_2O$, ammonium metavanadate NH_4VO_3, urea $CO(NH_2)_2$, APTES $C_9H_{23}NO_3Si$ and toluene C_7H_8, all materials were purchased from commercial sources (analytical grade) and used without further purification.

Instruments

The structure of the obtained $BiVO_4$ was confirmed by XRD measurement (XRDML) on sample stage = reflection-transmission Spinner PW3064/60; minimum step size Phi:0.1 diffractometer system = XPERT-PRo.

The morphology of the prepared samples was investigated *via* field-emission scanning electron microscope (FE-SEM, model: TeScan-Mira III Manufacturer, Czech). The Brunauer-Emmett-Teller (BET) surface areas of the samples were determined by nitrogen adsorption measurements using a Bel-Japan Minisorp II surface area and pore size analyzer. The adsorption-desorption isotherms were evaluated at -196 °C, once the samples were degassed at 120 °C for 24 h. The structure of the as-fabricated samples was measured by Fourier transform infrared spectrometer using pressed KBr pellets method (FTIR, FTIR-8400S SHIMADZU, Japan) and laser Raman spectrometer (Lab RAM HR Evolution Raman spectrometer HORIBA, France). Diffuse Reflectance UV-Vis spectroscopy (DRS) was applied to measure absorption of $BiVO_4$ by a Varian Cary 1E UV-Vis spectrophotometer equipped with a home-made spherical mirror device to concentrate diffuse reflection. A Kodak analytical $BaSO_4$ standard white reflectance coating was used as reference.

Catalysts Preparation

The $BiVO_4$ powders were prepared using a simple hydrothermal method. In a typical synthesis, 0.006 mol bismuth nitrate ($Bi(NO_3)_3{\cdot}5H_2O$), 0.006 mol ammonium metavanadate, (NH_4VO_3) and 0.4 g urea ($CO(NH_2)_2$) were dissolved in 30 ml deionized water under vigorous magnetic stirring, and then the pH of the resulting solution was adjusted to 1 with HNO_3 (65-68 wt%) solution. After stirring for 2 h, the suspension was transferred into a 50 ml Teflon-lined stainless-steel autoclave to perform hydrothermal process at 180 °C for 24 h. Once cooled down to room temperature, the solid product was collected through centrifugation (2000 rpm) and washed with deionized water for five times. The target $BiVO_4$ was finally obtained by drying at 60 °C for 12 h.

Surface Modification

Next, 0.05 g of $BiVO_4$ catalyst was added to 50 ml of

anhydrous toluene, followed by the addition of APTES to create solution concentrations of 10, 50 and 100 mM. The reaction was held at either 36, 70 and 90 °C under a heated water bath equipped with a return condenser. The reaction time was 3 and 8 h. After the completion of the reaction time, catalysts were removed from the APTES solution and rinsed under flowing toluene, after which acetone and ethanol catalysts were then dried at 70 °C.

Design of Experiment

Design of experiment is a method that results in a satisfactory result based on a limited number of observations. In this research, a complete factorial method was used. In this regard, response surface methodology (RSM) is used to model and analyze issues that are affected by multiple variables. In this study, RSM based on Box-Behnken designs with 4 variables was used to examine the relationship between the obtained responses and the process variables where the components were optimized by Design Expert software. The effects of independent variables including X_1 (concentration of pollutant (ppm)), X_2 (time (h)), X_3 (mass of catalyst (g)), and X_4 (concentration of hydrogen peroxide (M)) were evaluated at three levels, as shown in Table 1. The number of experiments was designed by Design Expert software 27 run, as shown in Table S1. The general equation of the response surface is defined as follows:

$$Y = \beta_0 + \sum_{j=1}^{k} \beta_j X_j + \sum_{j=1}^{k} \beta_{jj} X_j^2 + \sum_i \sum_{<j=2}^{k} \beta_{ij} X_i X_j + e_i \quad (1)$$

where Y is the predicted response (predicted adsorption capacity), X_i and X_j are the independent variables in coded levels, β_0 is the intercept, β_i, β_{jj}, β_{ij} are the linear, squared and interaction effect coefficients, respectively, k is the number of factors (independent variables) and e_i is the model error. The degradation efficiency of oily pollutant was calculated according to the following equation:

$$\text{Degradation efficiency } \% = \frac{(COD_0 - COD_f)}{COD_0} * 100\% \quad (2)$$

In this equation, COD_0 is the initial of chemical oxygen demand and COD_f is the final of chemical oxygen demand in the reaction.

Photocatalytic Degradation

Kerosene is one of the materials that is resistant to biological decomposition. In this study, the photocatalytic activities were determined by the degradation of kerosene aqueous solution under visible light irradiation in quartz photochemical reactor. Initially, it was sonicated for 15 min and kept in dark for 20 min to reach adsorption-desorption equilibrium under magnetic stirring before irradiation. Then, the photo-degradation process was carried out for 120 ml of the aqueous solution at ambient temperature under visible light (xenon lamp 400 w) according to Table S1. Finally, for separating the catalyst from oily pollutant, the samples were washed and centrifuged at 6000 rpm for 10 min.

RESULTS AND DISCUSSION

Characterization

The X-ray diffraction (XRD) patterns of the $BiVO_4$ photocatalyst are shown in Fig. 1. The results show that the synthesized photocatalysts are consistent with the standard spectra (JCPDS file no. 01-075-1866) [21]. The synthesized $BiVO_4$ was crystalline and had high purity.

The morphology of the prepared samples was investigated SEM as shown in Figs. 2a and b. The images represent a uniform with a diameter of about 200-500 nm.

According to the EDS diagram, the presence of Bi (58.90%), O(21.48%) and V (19.63%) elements in BiVO4/APTES confirms that, with the exception of these elements, no other element was found in the sample indicating the formation of a high purity $BiVO_4$/APTES (Fig. 2c).

The Brunauer-Emmett-Teller (BET) surface areas of the samples were determined by nitrogen adsorption measurements analyzer. Figure 3 displays the graph of adsorption/desorption isotherms for $BiVO_4$ and APTES/$BiVO_4$ photocatalysts. The result of BET/BJH analysis of $BiVO_4$ photocatalyst was found as follows: $a_s = 1.71$ m^2 g^{-1}, total pore volume = 0.02 cm^3 g^{-1} and average pore diameter = 48.74 nm. Also, the result of BET/BJH analysis of APTES/$BiVO_4$ photocatalyst was found as follows: $a_s = 21.75$ m^2 g^{-1}, total pore volume = 0.08 cm^3 g^{-1} and

Table 1. Independent Variables and their Levels in the Experiment

Independent variables	Coded symbols	Levels
Concentration of pollutant (ppm)	X_1	300, 450, 600
Time (h)	X_2	1, 2, 3
Mass of catalyst (g)	X_3	0.2, 0.6, 1
Concentration of of hydrogen peroxide (M)	X_4	0.05, 0.28, 0.5

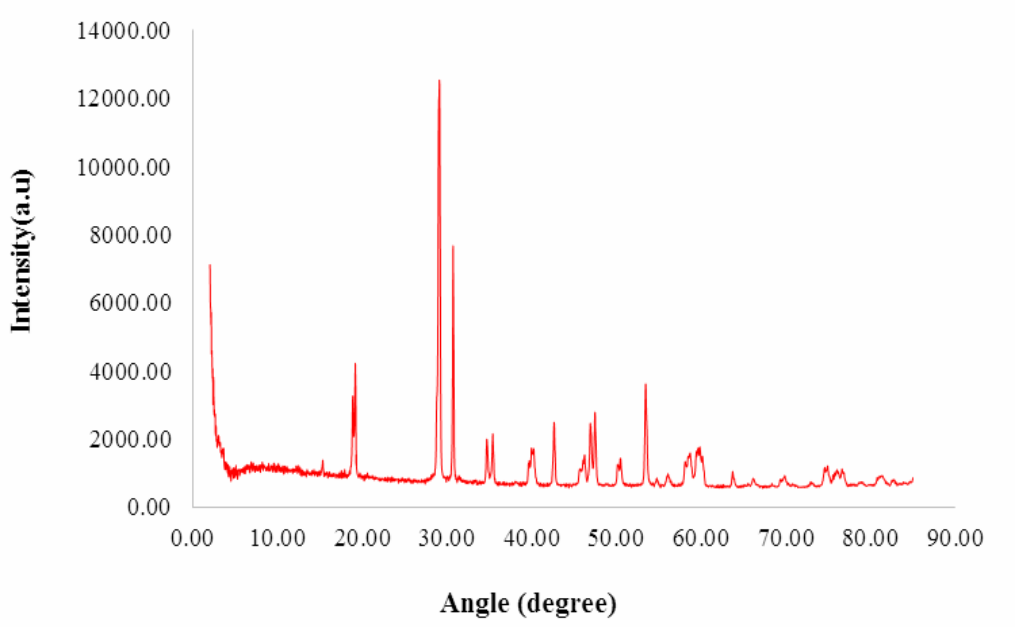

Fig. 1. X-ray diffraction pattern of $BiVO_4$.

average pore diameter = 27.32 nm. Based on the results, it can be concluded that the surface modification of $BiVO_4$ photocatalyst leads to increase in the surface area and total pore volume, while decrease in the mean pore diameter.

The infrared spectra of the $BiVO_4$ and $BiVO_4$/APTES photocatalysts are shown in Fig. 4. There are several peaks in $BiVO_4$/APTES, the most important of which are peaks within 1400 to 1700 cm^{-1} for hydroxylic group of BiOI/APTES. The peak at 1550 cm^{-1} for the NHCO groups is the result of the reaction between OH and NCO groups of isocyanate. The peaks within 1560 to 1605 cm^{-1} are related to the N-H bond in amines. The peak at 1629 cm^{-1} corresponds to the H-O-H bond of the water molecule. A very large peak in the range of 3200-3500 cm^{-1} belongs to the vibrations of the Si-OH groups due to the potential hydrolysis of the silane bonding compound. Multiple connections ranging from 2800-2900 cm^{-1} belong to the C-H bond on the CH_2 and C-H_3 groups. A wide range of wavelengths from 1,000-1,200 cm^{-1} belong to the Si-O and C-O heterogeneous ether attachments present in the silane amine bonding structure. The peak at 775 cm^{-1} is related to the vibrations of Si-O-CH_2 groups.

The TGA analysis was performed for samples and is shown in Fig. 5. The $BiVO_4$ and $BiVO_4$/APTES weight

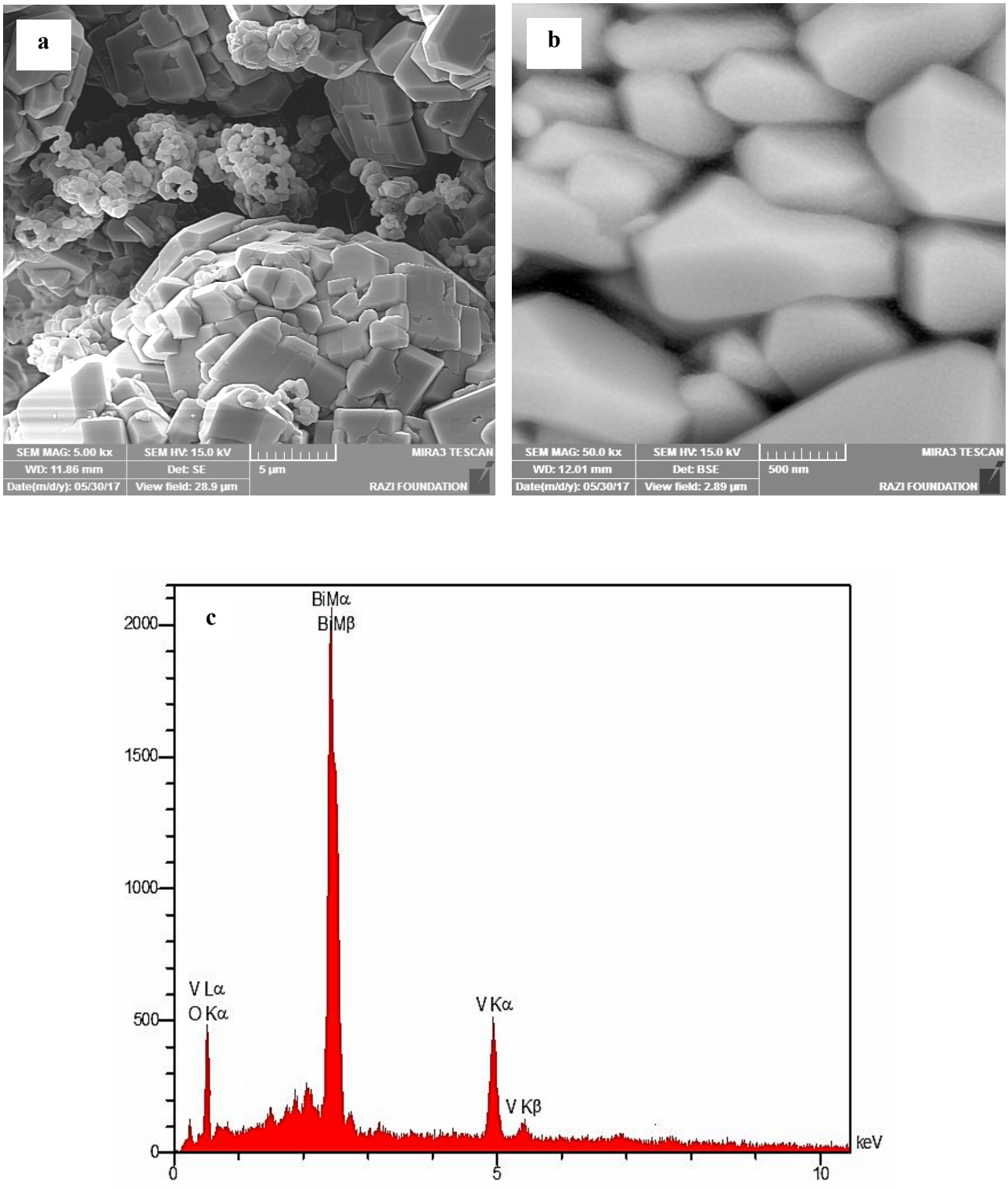

Fig. 2. SEM images of $BiVO_4$ with a) 5 µm and b) 500 nm resolution, and c) EDS diagram.

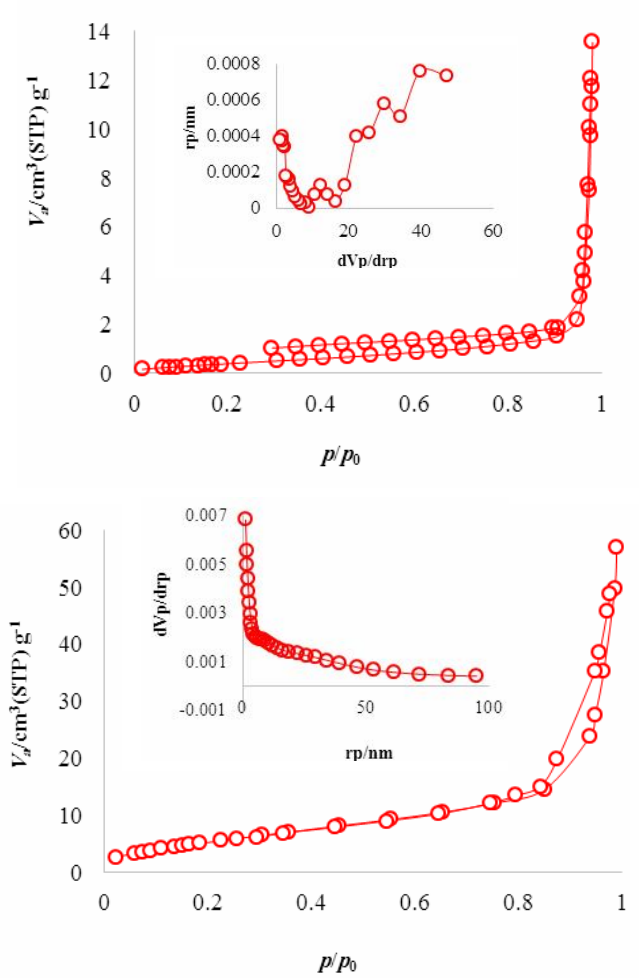

Fig. 3. N_2 adsorption-desorption isotherm and pore size distribution curve of a) $BiVO_4$ and b) APTES/$BiVO_4$.

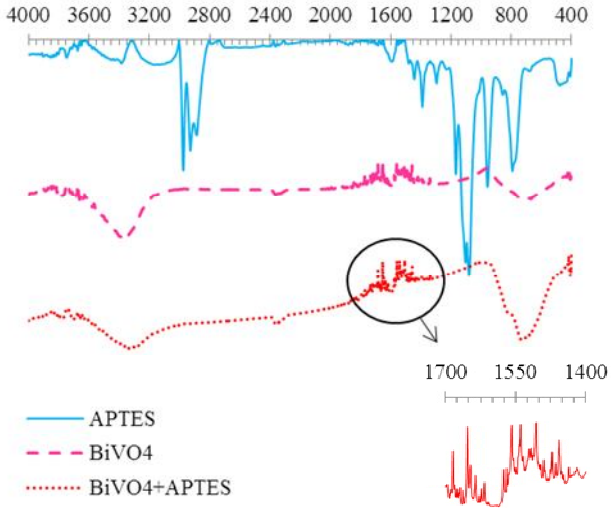

Fig. 4. FT-IR spectra of pure $BiVO_4$, and pure APTES and APTES/$BiVO_4$.

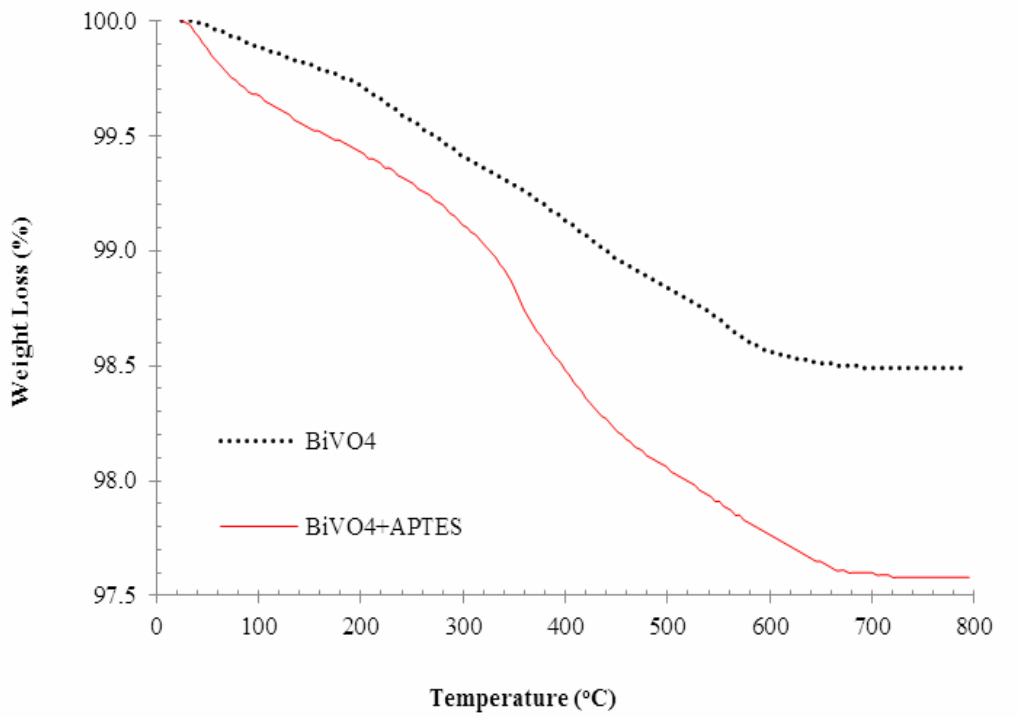

Fig. 5. TGA analysis of $BiVO_4$ and $BiVO_4$/APTES.

decreased by increasing temperature, caused by the release of different materials at different times. $BiVO_4$/APTES claims about 2.5% of weight loss, which can be attributed to binding of APTES on the surface. The weight loss within the temperature range of 350-450 °C is more severe, which can be attributed to the destruction of the organic/mineral silane groups. It can be concluded that the binding of APTES molecules to the surface of $BiVO_4$ molecules has been successful.

To determine the degree of hydrophobicity and hydrophilicity of surface, water contact angle test (WCA) was performed. The contact angle of the equilibrium indicates the relative strength of the molecular molecule of the liquid-solid and vapor. Contact angle measurement was performed with a drop of water (4 µl) with a system equipped with a droplet shooting camera (CCD) plus a droplet contact angle measurement software with the desired level. To examine the hydrophobicity property of $BiVO_4$ and $BiVO_4$/APTES, contact angle analysis was performed. As seen in Fig. 6. The contact angle of the $BiVO_4$ catalyst is 7.9, while after surface modification by APTES, the contact angle is equal to 46.5. Thus, the hydrophobicity of the $BiVO_4$ catalyst has increased after surface modification.

The method that is widely used to determine band gap is the Tauc diagram, which is used to obtain a band gap based on reflection spectra. The equation is as follows:

$$(\alpha h\nu)^{1/n} = A\,(h\nu - E_g) \quad (3)$$

where h is the Planck constant, ν represents the applied frequency, α is the absorption coefficient, E_g denotes the band gap, and A is a proportional constant. In addition, the band gap of $BiVO_4$ and $BiVO_4$/APTES was calculated as 2.36 and 2.06, respectively, as shown in Fig. 7.

Kinetic Experiments

The kinetics of adsorption requires the data on the amount of matter absorbed over time. Accordingly, we performed the following experiments. First, 0.05 g of $BiVO_4$/APTES was added to 100 ml of oily pollutant at a concentration of 670 mg l^{-1}, and stirred for 15, 30, 60, 120

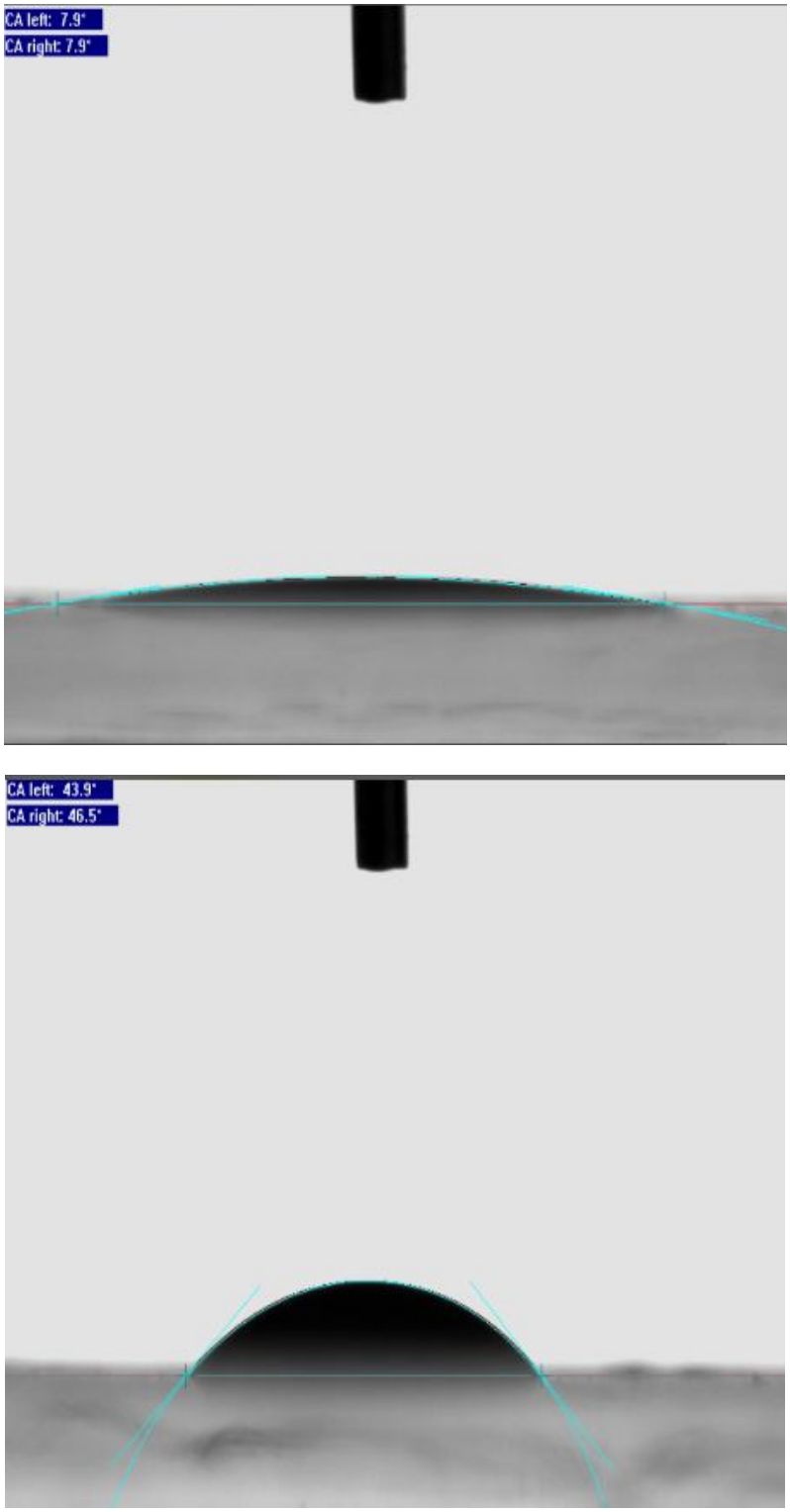

Fig. 6. CA analysis of a) $BiVO_4$ and b) $BiVO_4$/APTES.

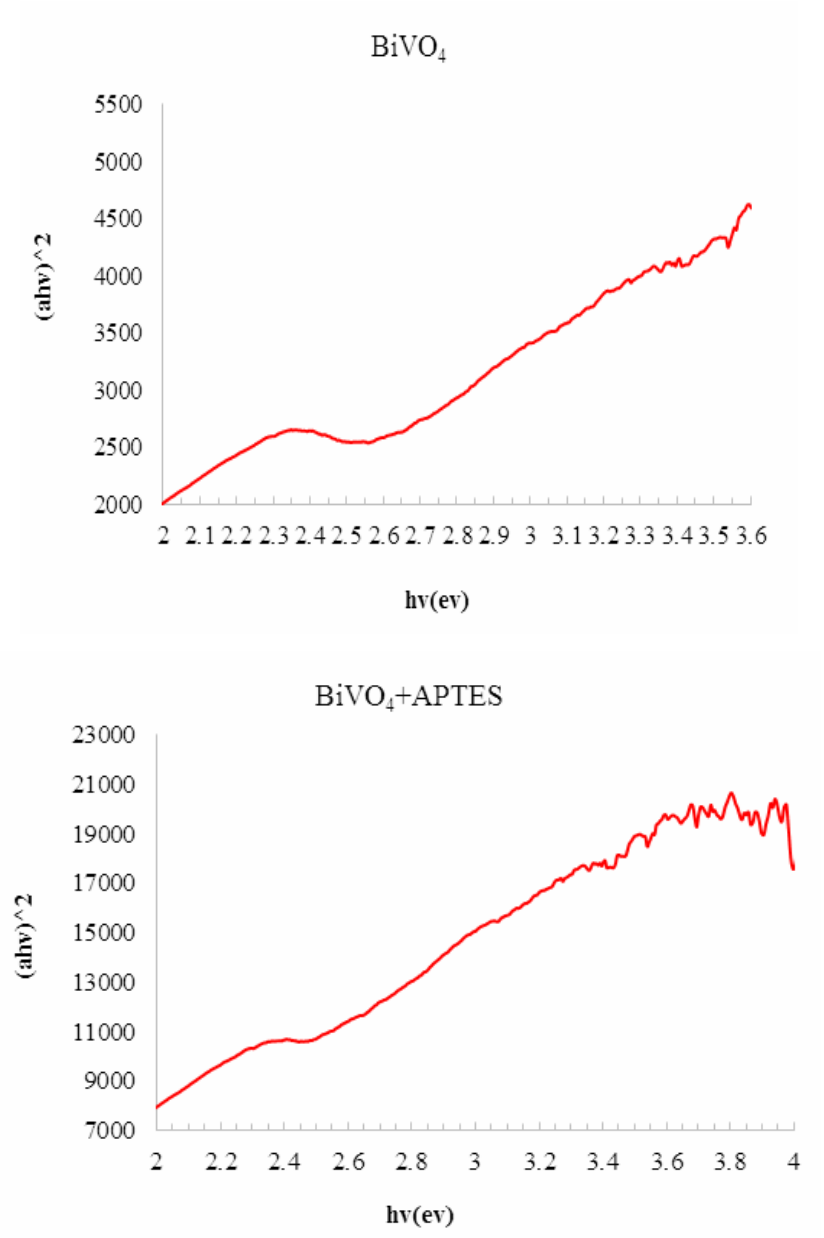

Fig. 7. Band gap of $BiVO_4$ and $BiVO_4$/APTES.

and 180 min at room temperature in the dark. Then, for separating the catalyst from oily pollutant, the samples were centrifuged at 6000 rpm for 10 min. In order to determine oily pollutant adsorption percentage, the initial and final COD was measured by COD-meter. The oily pollutant used in this research was kerosene (Fig. 8).

In this research, pseudo-first order and pseudo-second order kinetics were considered; hence, 180 min was divided into 7 intervals with the kinetic experiments conducted as follows. First, 100 ml of oily pollutant with concentration of 400 ppm, with 0.6 g of catalyst was poured into a quartz cell, after which oxidant was added and placed in the photoreactor under visible light exposure and sampled at different times.

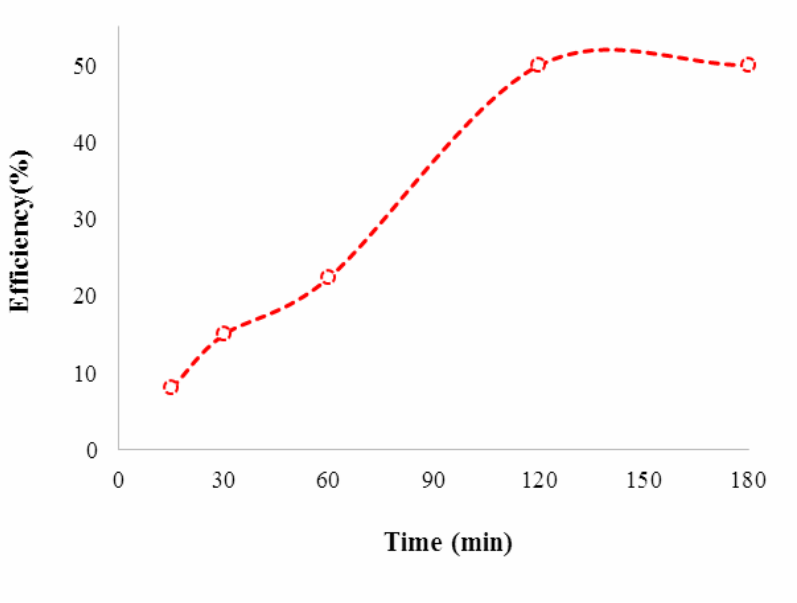

Fig. 8. Adsorption graph in time.

Thermodynamic Experiments

It is possible to obtain the equilibrium constant of reaction and photocatalyst adsorption capacity from thermodynamic data. There is a thermodynamic equilibrium between the mass of pollutant adsorbed per unit mass of adsorbent (q_e) and final concentrations of pollutant (c_e) at constant temperature and pH. In this research, experiments showed that oil is absorbed on a single-layer catalyst surface. The photocatalytic degradation of oil pollutants was carried out by $BiVO_4$ and $BiVO_4$/APTES under visible light irradiation with two-parameter isothermic equations such as Langmuir, Freundlich, Tempkin, and Dubinin-Radushkevich, with three parameters such as Redlich-Peterson, Khan, Radke-Prausnitz, and four parameters such as Fritz Shelander fitted [22]. Nonlinear fittings of the parameters of the calculated equations and their correlation coefficients were obtained. Isotherms are shown in Table 2. Specifically, 0.6 g of the catalyst was added to 100 ml of solution, placed on a magnetic stirrer for 60 min under a visible light. Then, the final concentration was determined. Using Eq. (4) and the equations in Table 2, q_e values were calculated and plotted against C_e and other parameters.

$$q_e = \frac{V(C_o - C_e)}{W} \quad (4)$$

where q_e is the mass of pollutant adsorbed per unit mass of adsorbent, and C_0 and Ce denote the initial and final concentrations, respectively. V is the volume of solution (L), and W shows the catalyst mass (g).

The Surface Modification with Different Conditions

Table 3 shows the effects of APTES concentration (mM), temperature (°C) and time (h) on the surface modification. Based on the results, the highest degradation efficiency is related to the APTES/$BiVO_4$ photocatalyst with a concentration of 100 mM, temperature of 90 °C and time of 8 h.

The Effect of Surface Modification on Hydrophobicity, Band Gap, Irradiation Type and Efficiency

Table 4 shows that the efficiency of oily pollutant degradation increased using $BiVO_4$/APTES, compared to $BiVO_4$, by about 5.6%. Adding silicon materials to metal oxides can increase the hydrophobicity of the metal oxide surface, so case more pollutant molecules will adsorb to this surface, leading to CO_2 and H_2O. Also, the efficiency of the degradation of oily pollutant from the aqueous solution by the $BiVO_4$/APTES increased by visible light compared to

Table 2. Lists of Adsorption Isotherms Models

Isotherm	Nonlinear form	Isotherm	Nonlinear form	Isotherm	Nonlinear form
2 Parameters		3 Parameters		4 Parameters	
Langmuir	$q_e = \frac{q_m b_L C_e}{1 + b_L C_e}$	Redlich-Peterson	$q_e = \frac{K_R C_e}{1 + a_R C_e^g}$	Fritz-Schlunder	$q_e = \frac{CC_e^{\alpha_{FS}}}{1 + DC_e^{\beta_{FS}}}$
Freundlich	$q_e = K_f C_e^{1/n}$	Khan	$q_e = \frac{q_S b_{KH} C_e}{(1 + b_{KH} C_e)^{a_{KH}}}$		
Tempkin	$q_e = B_T \ln A_T C_e$	Radke-Prausnitz	$q_e = \frac{a_{RP} r_{RP} C_e}{1 + r_R C_e^{B_{RP}}}$		
Dubinin-Radushkevich	$q_e = q_s \exp(-k_{ad}\varepsilon^2)$				
Volmer	$C_e = \frac{\theta_V}{d(1-\theta_V)} \exp\left(\frac{\theta_V}{1-\theta_V}\right)$				

Table 3. The Effect of APTES Concentration, Temperature and Time on Surface Modification in Efficiency

Experiment	Catalyst	APTES of concentration (mM)	Temperature (°C)	Time (h)	Degradation (%)
1	$BiVO_4$+ APTES	10	36	3	62.25
2	$BiVO_4$ + APTES	50	70	8	72.43
3	$BiVO_4$+ APTES	100	90	8	79.6

the UV light, as the energy of the lower band gap can be provided by visible light. This can be considered as a desirable result due to the disadvantages of using UV light and its damages for humans and the environment. The results obtained from experiments performed by $BiVO_4$, $BiVO_4$/APTES are shown Table 5. The results BET of the modified photocatalyst (APTES/ $BiVO_4$) are shown in Fig. 3b). According to the results, the surface area increases with the surface modification and the degradation efficiency increases with increasing surface area.

Effect of Pollutant Concentration on Efficiency

According to Table 6, the efficiency of the degradation of oily pollutant from the aqueous solution by

Table 5. The Effect of Surface Modification on Band Gap and on Efficiency

Experiment	Catalyst	Band gap (ev)	Type of light	Degradation (%)
1	$BiVO_4$	2.36	Visible	74
2	$BiVO_4$	2.36	UV-C	76
3	$BiVO_4$ + APTES	2.06	Visible	79.6

Table 6. The Effect of Pollutant Concentration on Efficiency

Experiment	Catalyst	Pollutant concentration ($mg\ l^{-1}$)	Degradation (%)
1	$BiVO_4$ + APTES	11	26.5
2	$BiVO_4$ + APTES	22	45.8

Table 7. The Effect of Concentration of Hydrogen Peroxide on Efficiency

Experiment	Catalyst	Concentration of hydrogen peroxide (M)	Degradation (%)
1	$BiVO_4$ + APTES	0.05	55.8
2	$BiVO_4$ + APTES	0.5	10.2

Table 8. The Effect of Catalytic Mass on Efficiency

Experiment	Catalyst	Catalytic mass (g)	Degradation (%)
1	$BiVO_4$ + APTES	0.2	28.2
2	$BiVO_4$ + APTES	1	64.6

Table 9. The Effect of Reaction Time on Efficiency

Experiment	Catalyst	Reaction time (h)	Degradation (%)
1	$BiVO_4$ + APTES	1	10.2
2	$BiVO_4$ + APTES	3	79.6

$BiVO_4$/APTES increases by doubling the pollutant concentration by about 19.3%, as doubling the pollutant concentration increases the number of molecules that collide with the surface and absorb on the surface.

Effect of Concentration of Hydrogen Peroxide on Efficiency

In general, the hydrogen peroxide enters the experiment media to facilitate degradation. Increased hydrogen peroxide is one of the factors accelerating the degradation process, but this increase is somewhat effective and more than that plays a destructive role in degradation, because excess hydrogen peroxide can act as a radical trap for $OH^{\bullet}$ and reduce the rate of degradation. According to the results (Table 7), with increasing hydrogen peroxide concentration from 0.05 to 0.5 M, the degradation efficiency decreases from 55.8 to 10.2%.

Effect of Catalytic Mass on Efficiency

Table 8 indicates that the efficiency of the degradation of oily pollutant from the aqueous solution by the $BiVO_4$/APTES increases by about 36.4% with 5-fold increase in the catalytic mass, since enhancing the catalytic mass increases active sites.

Effect of Reaction Time on Efficiency

Table 9 reveals that the efficiency of the degradation of oily pollutant from the aqueous solution by the $BiVO_4$/APTES increases by about 69.4% with a 3-fold increase in reaction time, since increasing the reaction time increases the encounter time of the molecules.

Effect of Photocatalyst Regeneration on Efficiency

According to Table 10, the efficiency of the degradation of oily pollutant from the aqueous solution by the $BiVO_4$/APTES decreases after every use and recovery, indicating that the recovery mechanism of this catalyst may not be appropriate and other methods should be used. The results of the experiments designed by the Box-Behnken method are shown in Table S1.

According to the experimental conditions provided by the software, the highest percentage of degradation was obtained as 79.6% for $BiVO_4$/APTES. Normalization is the basic precondition of multivariate analysis. If this assumption does not exist, some of the specific statistical tests are invalid and cannot be used. Figure 9 displays the assumption of the normalization of the data which is almost normal with the results, showing how the residues follow a normal distribution. This shows a very good correlation between the results obtained by the experimental method and the values predicted by the statistical method. One of the most widely used tools in the hypothesis test and statistical research is "Analysis of Variance". This method attempts to assess the parameters. The results of ANOVA are shown in Table S2.

In Table S2, quadratic model is significant, indicating that the selected model is a suitable model for data. Statistical studies are performed at 95% confidence level (alpha = 0.05). At 95% confidence level, if the P-value is smaller than 0.05, they will reject the null hypothesis, otherwise the null hypothesis is accepted. Among the factors, time, concentration of pollutant, concentration of H_2O_2, and mass of catalyst are influential, respectively. Figure 10 shows the effect of mass of catalyst g and time h. Figure 11 depicts the effect of concentration of H_2O_2 M and time h. Figure 12 indicates the effect of mass of catalyst g and concentration of H_2O_2 M in the photocatalytic degradation, as (a) contour plot and (b) 3D model. Based on the results, it can be concluded that time factor is the most effective factor, while hydrogen peroxide has a lesser impact on degradation of oily pollutant. Finally, the software is the best point for achieving the highest percentage of degradation of oily pollutant under optimal conditions with pollutant concentration of 436.32 ppm, time of 2.62 h, catalyst mass of 0.77 g and H_2O_2 concentration of 0.42 M, with desirability 1, where the highest percentage of degradation was obtained as 79.6% (Fig. 13).

The experimental data were fitted with different isotherms and the results are shown in Table S3. Experimental kinetic data were fitted with Logergern, Elovich, Blanchard, and intra-particle diffusion control models and the results are shown in Table S4.

CONCLUSIONS

In the present work, $BiVO_4$ photocatalyst was synthesized by a simple hydrothermal method. In order to

Table 10. The Effect of Regeneration on Efficiency

Experiment	Catalyst	Number of regeneration	Degradation (%)
1A	$BiVO_4$ + APTES	0	78.4
1B	$BiVO_4$ + APTES	1	58
1C	$BiVO_4$ + APTES	2	48

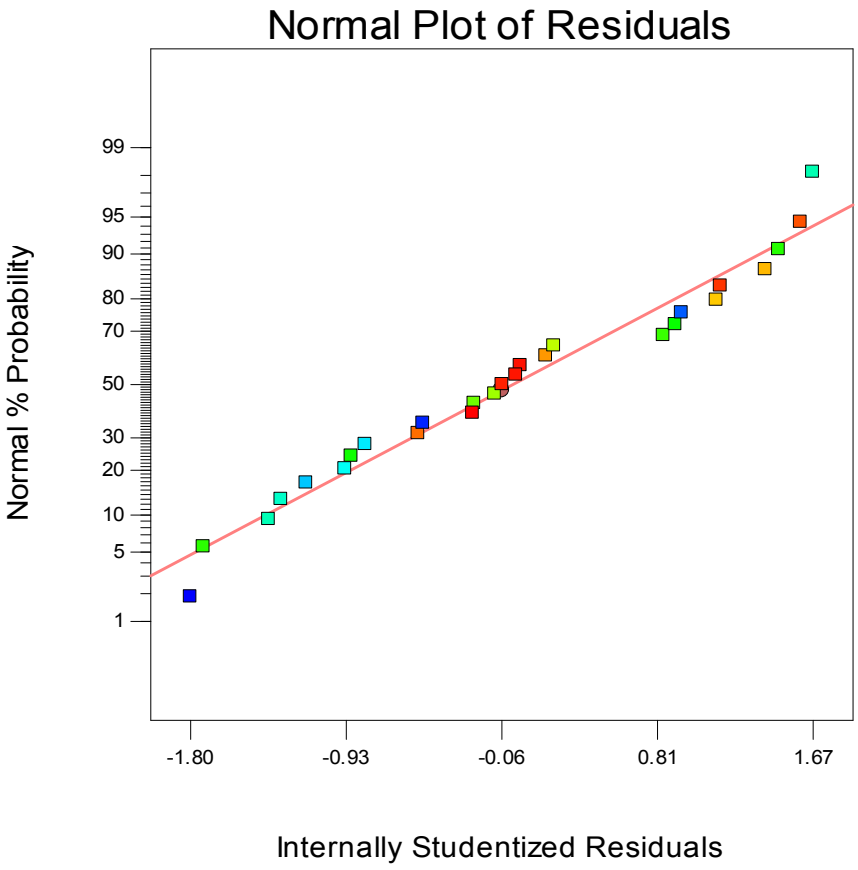

Fig. 9. Normal probability plot of the studentized residual for photodegradation of oily pollutant.

enhance its hydrophobicity, its surface was modified by APTES. Box-Behnken method was used to optimize the photocatalytic degradation conditions. $BiVO_4$ and $BiVO_4$/APTES were compared for hydrophobicity, band gap, and the effect of parameters. The degradation of oily pollutant was obtained as 79.6% under optimal conditions with pollutant concentration of 436.32 ppm, time of 2.62 h, catalyst mass of 0.77 g and H_2O_2 concentration of 0.42 M. The photocatalytic activities were evaluated on the degradation of kerosene. It was found that the optimizing activity of $BiVO_4$ is improved through its modification. Isothermic studies revealed that linear Langmuir and

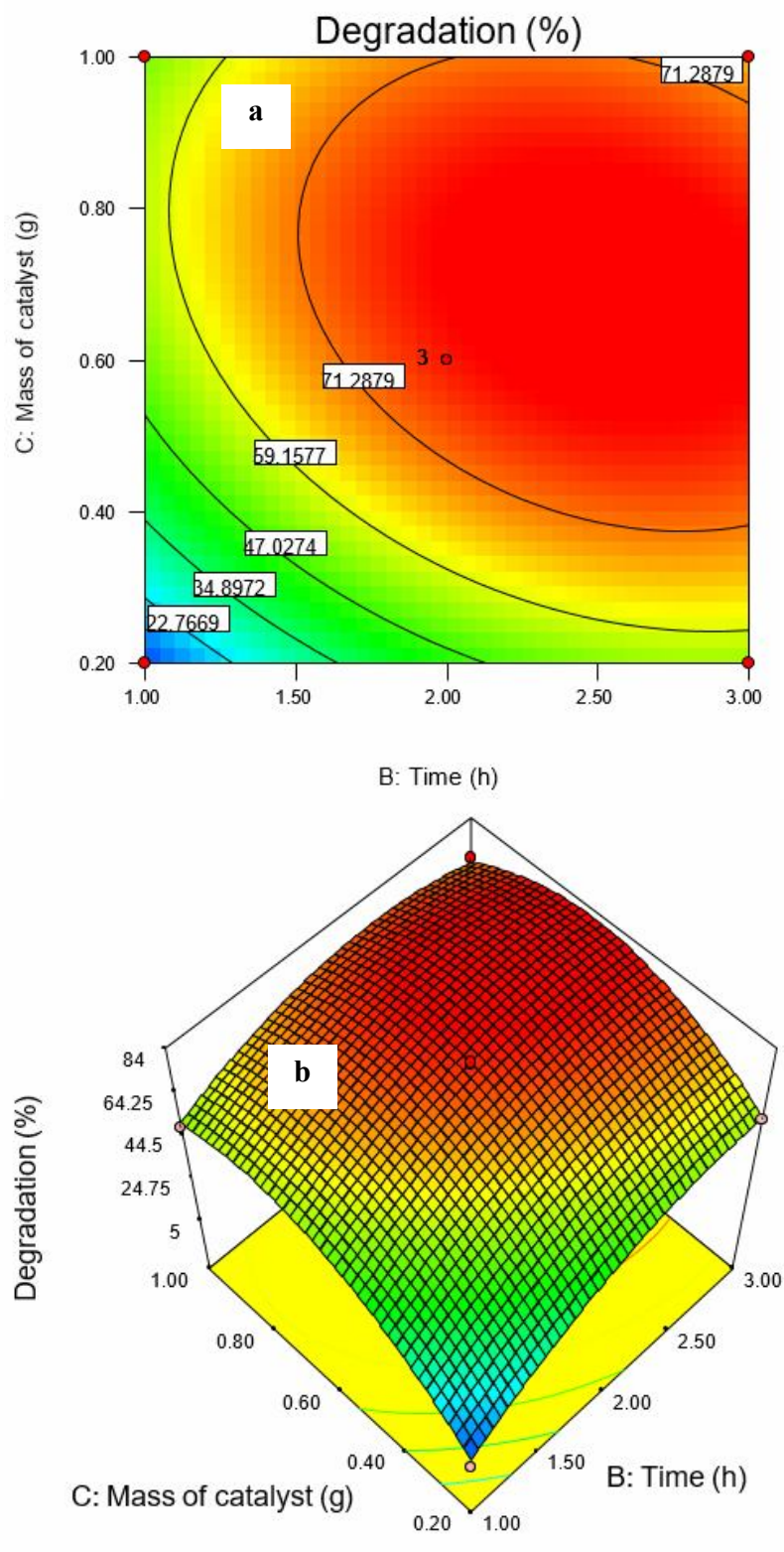

Fig. 10. a) Contour and b) 3D plots for efficiency as a mass of catalyst and time.

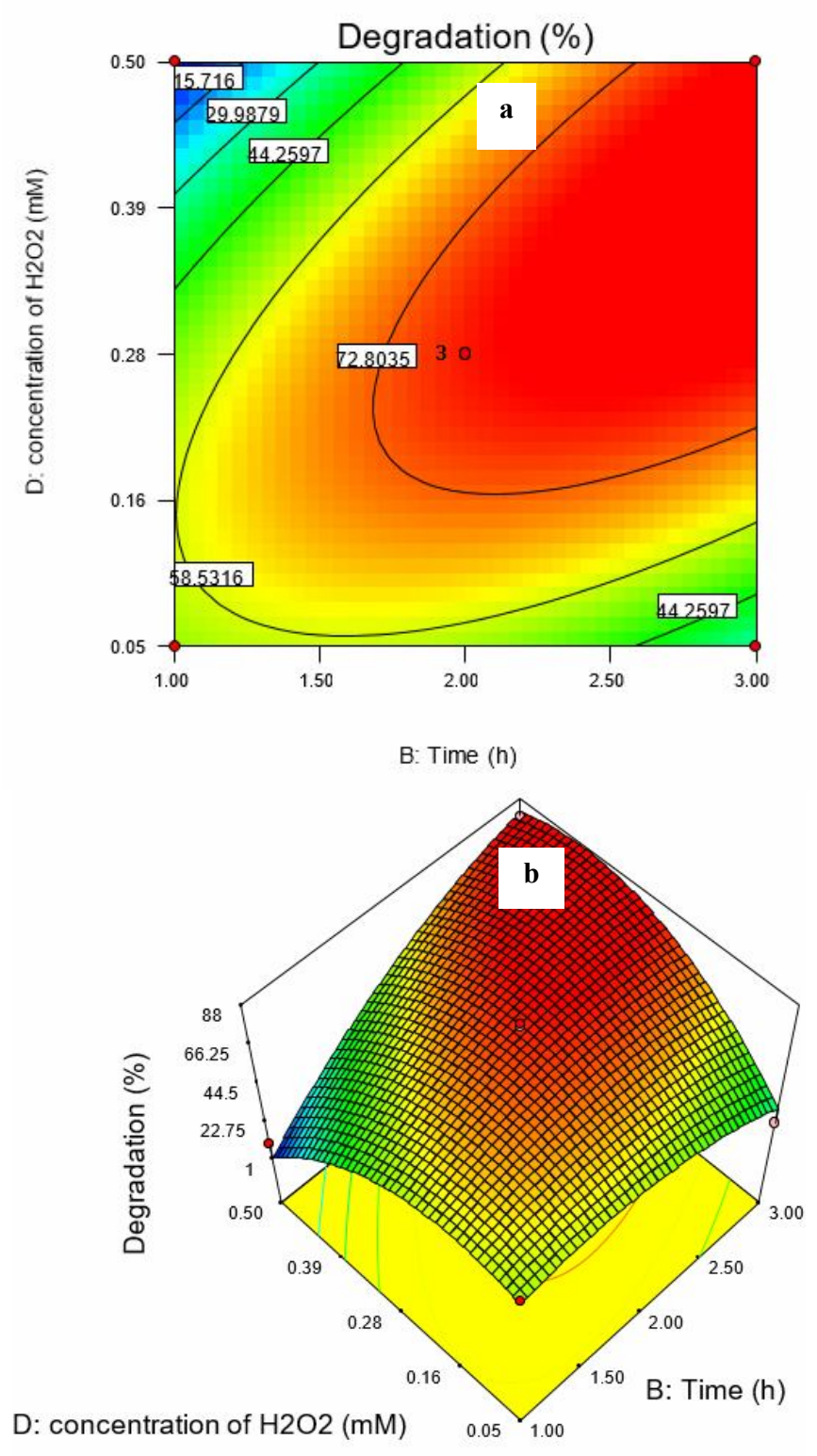

Fig. 11. a) Contour and b) 3D plots for efficiency as a concentration of hydrogen peroxide and time.

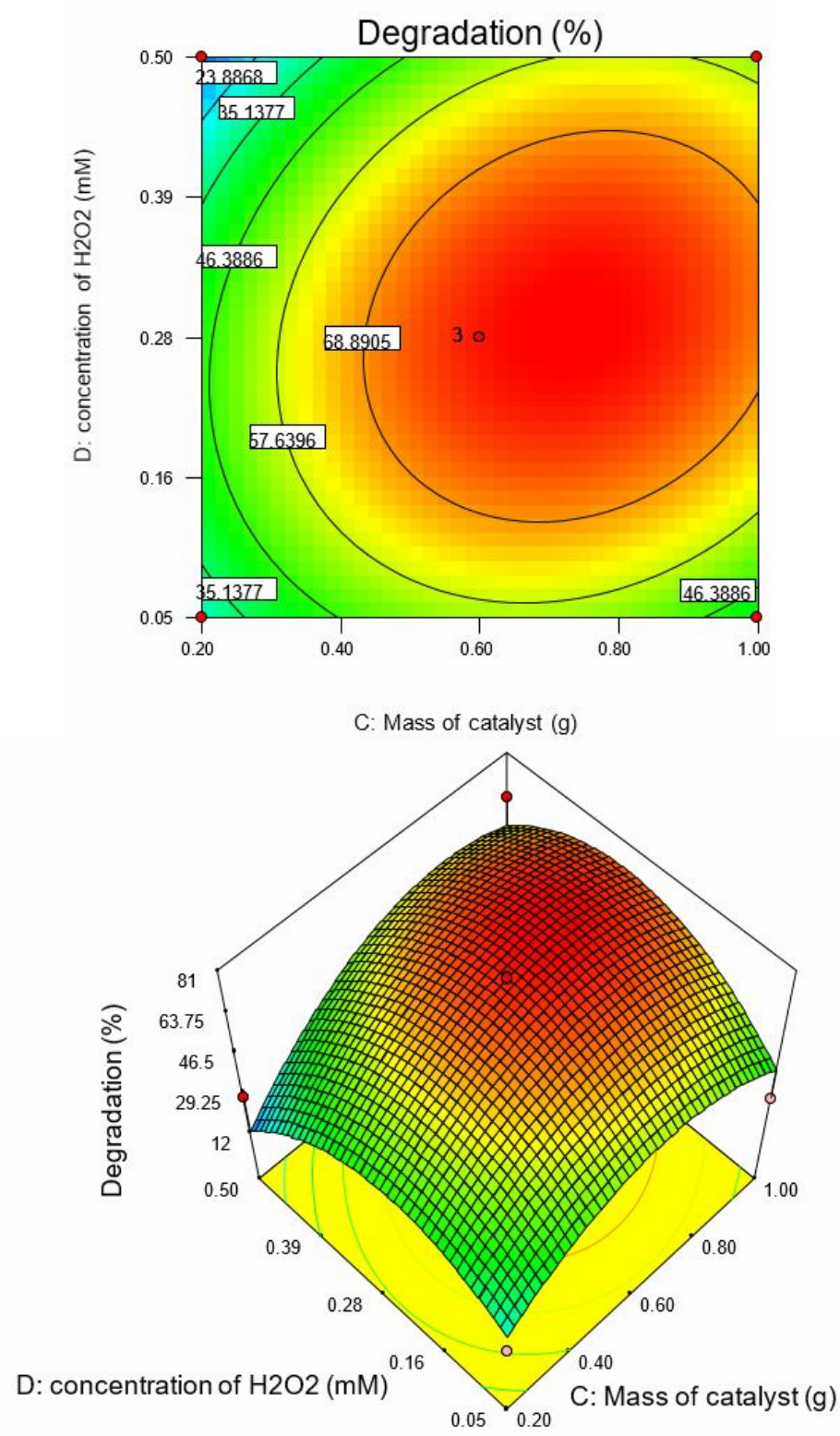

Fig. 12. a) Contour and b) 3D plots for efficiency as a concentration of hydrogen peroxide and mass of catalyst.

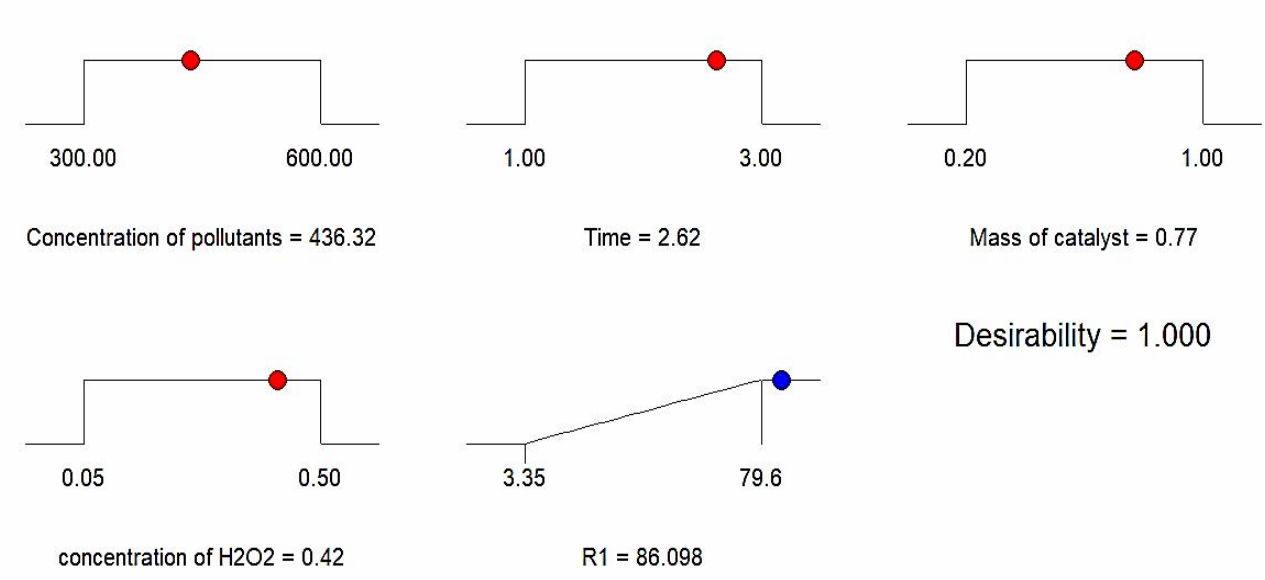

Fig. 13. Graphs of the optimum conditions for photodegradation of oily pollutant.

Freundlich and non-linear Volmer isotherms have the best fit with $BiVO_4$ and $BiVO_4$/ATPES data, respectively. The results showed that the intra-particle diffusion control kinetic equation has the largest correlation coefficient.

REFERENCES

[1] Sun, S.; Wang, W., Advanced chemical compositions and nanoarchitectures of bismuth based complex oxides for solar photocatalytic application. *RSC. Adv,* **2014**, *4*, 47136-47152. DOI: 10.1039/C4RA06419D.

[2] Abdolmohammadi, S.; Shariati, S.; Fard, N. E.; Samani, A., Aqueous-mediated green synthesis of novel spiro [indole-quinazoline] derivatives using kit-6 mesoporous silica coated Fe_3O_4 nanoparticles as catalyst. *J. Hetero. Chem.,* **2020**, *5*, 2729-2737. DOI: 10.1002/jhet.3981.

[3] Fard, N. E.; Fazaeli, R., A novel kinetic approach for photocatalytic degradation of azo dye with CdS and Ag/CdS nanoparticles fixed on a cement bed in a continuous-flow photoreactor. *International J. Chem. Kin,* **2016**, *48*, 691-701. DOI: 10.1002/ kin.21025.

[4] Fard, N. E.; Fazaeli, R.; Yousefi, M.; Abdolmohammadi, S., Morphology-controlled synthesis of CuO, CuO rod/MWW composite for advanced oxidation of indole and benzothiophene. *Chem. Select,* **2019**, *4*, 9529-9539. DOI: 10.1002/slct.201901514.

[5] Fard, N. E.; Fazaeli, R.; Yousefi, M.; Abdolmohammadi, S., Oxidation of carbazole by shape-controllable Cu_2O on MWW catalysis. *Appl. Physic. A,* **2019**, *125*, 632. DOI: 10.1007/s00339-019-2918-9.

[6] Abdolmohammadi, S., Solvent-free synthesis of 4, 5-dihydropyrano [c] chromene derivatives over TiO2 nanoparticles as an economical and efficient catalyst. *Current. Catal.,* **2013**, *2*, 116-121. DOI: 10.2174/2211544711302020005.

[7] Rashidi, S.; Nikazar, M.; Yazdi, A. V.; Fazaeli, R., Optimized photocatalytic degradation of Reactive Blue 2 by TiO_2/UV process. *J. Environ. Sci. Health, Part A*, **2014**, *49*, 452-462. DOI: 10.1080/ 10934529.2014.854685.

[8] Elmi Fard, N.; Fazaeli, R., Experimental design study of RB 255 photocatalytic degradation under visible light using synthetic Ag/TiO_2 nanoparticles: Optimization of experimental conditions. Iran. J. Catal., **2018**, 8, 133-141.

[9] Fard, N. E.; Fazaeli, R., Optimization of operating parameters in photocatalytic activity of visible Light active Ag/TiO_2 nanoparticles. *Russ. J. Physic. Chem. A,* **2018**, *92*, 2835-2846. DOI: 10.1134/S0036024418130071.

[10] Malathi, A.; Madhavan, J.; Ashokkumar, M.; Arunachalam, P., A review on $BiVO_4$ photocatalyst: activity enhancement methods for solar photocatalytic applications. *Appl. Catal. A: Gen.,* **2018**, *555*, 47-74. DOI: 10.1016/j.apcata.2018.02.010.

[11] Zhao, Y.; Li, R.; Mu, L.; Li, C., Significance of crystal morphology controlling in semiconductor-based photocatalysis: a case study on $BiVO_4$ photocatalyst. *Cryst. Growth. Des*., **2017**, *17*, 2923-2928. DOI: 10.1021/acs.cgd.7b00291.

[12] Zhang, Y.; Park, S. J., Au-pd bimetallic alloy nanoparticle-decorated $BiPO_4$ nanorods for enhanced photocatalytic oxidation of trichloroethylene. *J. Catal.,* **2017**, *355*, 1-10. DOI: 10.1016/j.jcat.2017.08.007.

[13] Pirhashemi, M.; Habibi-Yangjeh, A.; Pouran, S. R., Review on the criteria anticipated for the fabrication of highly efficient ZnO-based visible-light-driven photocatalysts. *J. Ind. Eng. Chem.,* **2018**, *62*, 1-25. DOI: 10.1016/j.jiec.2018.01.012.

[14] Akhundi, A.; Habibi-Yangjeh, A.; Abitorabi, M.; Rahim Pouran, S., Review on photocatalytic conversion of carbon dioxide to value-added compounds and renewable fuels by graphitic carbon nitride-based photocatalysts. *Catal. Rev.,* **2019**, *61*, 595-628. DOI: 10.1080/01614940.2019.1654224.

[15] Akhundi, A.; Badiei, A.; Ziarani, G. M.; Habibi-Yangjeh, A.; Muñoz-Batista, M. J.; Luque, R., Graphitic carbon nitride-based photocatalysts: Toward efficient organic transformation for value-added chemicals production. *Mol. Catal.,* **2020**, *488*, 110902. DOI: 10.1016/j.mcat.2020.110902.

[16] Asadzadeh-Khaneghah, S.; Habibi-Yangjeh, A., g-C_3N_4/carbon dot-based nanocomposites serve as efficacious photocatalysts for environmental purification and energy generation: A review. *J. Clean. Prod.,* **2020**, *276*, 124319. DOI: 10.1016/j.jclepro.2020.124319.

[17] Katoueizadeh, E.; Zebarjad, S. M.; Janghorban, K., Morphological study of surface-modified urea-formaldehyde microcapsules using 3-aminopropyl-triethoxy silane. *Polymer. Bulletin,* **2019**, *76*, 1317-1331. DOI: 10.1007/s00289-018-2425-8.

[18] Nakaramontri, Y.; Nakason, C.; Kummerlöwe, C.; Vennemann, N., Enhancement of electrical conductivity and other related properties of epoxidized natural rubber/carbon nanotube composites by optimizing concentration of 3-aminopropyltriethoxy silane. *Poly. Eng. Sci.,* **2017**, *57*, 381-391. DOI: doi.org/10.1002/pen.24433.

[19] Fazaeli, R.; Fard, N. E., Desulfurization of gasoline fuel *via* photocatalytic oxidation/adsorption using NaX zeolite-based under mild conditions: Process optimization by central composite design. *Russ. J. Appl. Chem.,* **2020**, *93*, 973-982. DOI: 10.1134/S1070427220070058.

[20] Kashi, N.; Fard, N. E.; Fazaeli, R., Empirical modeling and CCD-based RSM optimization of Cd(II) adsorption from aqueous solution on clinoptilolite and bentonite. *Russ. J. Appl. Chem.*, **2017**, *90*, 977-992. DOI: 10.1134/S1070427217060210.

[21] Pookmanee, P.; Pingmuang, K.; Kangwansupamonkon, W.; Phanichphant, S., Methylene blue degradation over photocatalyst bismuth vanadate powder synthesized by the hydrothermal method. *Adv. Mater. Res.,* **2010**, *93*, 177-180. .DOI: 10.4028/www.scientific.net/AMR.93-94.177.

[22] Saadi, R.; Saadi, Z.; Fazaeli, R.; Fard, N. E., Monolayer and multilayer adsorption isotherm models for sorption from aqueous media. *Korea. J. Chem. Eng.,* **2015**, *32*, 787-799. DOI: 10.1007/s11814-015-0053-7.